Quantum Monte Carlo study of the attractive kagome-lattice Hubbard model

Xingchuan Zhu [1], Wanpeng Han [2], Shiping Feng [3], and Huaiming Guo [2,*]

[1] *Interdisciplinary Center for Fundamental and Frontier Sciences, Nanjing University of Science and Technology, Jiangyin, Jiangsu 214443, China*

[2] *School of Physics, Beihang University, Beijing 100191, China*

[3] *Department of Physics, Beijing Normal University, Beijing 100875, China*

(Received 15 December 2022; revised 21 February 2023; accepted 16 March 2023; published 19 April 2023)

The recent experimental discovery of several families of kagome materials has boosted the interest in electronic correlations on a kagome lattice. As an initial step to understand the observed complex phenomena, it is helpful to know the correspondence between the simple forms of interactions and the induced correlated states on a kagome lattice. Considering the lack of such studies, here we systematically investigate the attractive kagome-lattice Hubbard model using the mean-field approach and determinant quantum Monte Carlo (DQMC). A charge-density-wave order satisfying the triangle rule is predicted by the mean-field treatment, and subsequent DQMC simulations provide indirect evidence for its existence. The *s*-wave superconductivity is found to be stabilized at low temperatures, and to exist in dome regions of the phase diagrams. We then determine the superconducting critical temperature quantitatively by finite-size scaling of the pair structure factor. These results may be helpful in understanding the observed superconductivity in kagome materials.

DOI: 10.1103/PhysRevResearch.5.023037

I. INTRODUCTION

The kagome lattice, formed by corner-sharing triangles, is unique in that it combines the intriguing physics of geometry frustration, and flat band and Dirac fermions, and thus sets an ideal platform for novel quantum phases [1]. Due to the strong geometry frustration, the antiferromagnetic spin-1/2 Heisenberg model on the kagome lattice is a paradigmatic realization of a quantum spin liquid (QSL). Many efforts have been devoted to uncover its physical nature, among a gapless $U(1)$ Dirac QSL, a gapped topological Z_2 QSL, and chiral QSL [2–7]. The rich features in the energy dispersion of the itinerant electrons on the kagome lattice have provoked great interest in investigating the exotic quantum orders of fermions. Especially, spin-orbit coupling can open a nontrivial gap at the Dirac point and the quadratic band crossing point touching the flat band, generating Z_2 topological insulating states [8]. Remarkably, several magnetically ordered materials that contain a kagome lattice have been found recently, and the experimental evidence points to the realization of the above simple topological model [9–13]. Theoretically, a rich variety of interaction-driven phases have been proposed, including a dynamically generated topological phase, various spin or charge bond orders and density waves [14–17], and the superconducting instability [18–21].

The interest in electronic correlations in a kagome lattice is further boosted by the recent experimental discovery of several families of kagome materials, such as T_mX_n (T = Fe, Co and X = Sn, Ge) and AV_3Sb_5 (A = Cs, K, Rb) [9,10,22]. The exhibited topological quantum states and a cascade of correlated phases have received significant research interest [23–25]. Specifically, in the new kagome prototype materials AV_3Sb_5 (A = Cs, K, Rb), a stacked ideal kagome network of vanadium layers gives rise to rich correlated electronic phases including charge-density-wave (CDW) order occurring below $T_c^{\rm CDW} \approx$ 80–110 K, a further transition at $T' = 35$ K with an additional unidirectional charge ordering vector, and unconventional superconductivity with critical temperatures $T_c \approx$ 0.9–2.7 K [26]. The CDW order, which may be closely related to van Hove singularities at the Fermi level [27], exhibits exotic characteristics such as time-reversal symmetry breaking [28–30] and nematicity [31]. Its interplay with superconductivity has been investigated by applying external pressure. As the CDW is destabilized by pressure, the superconducting state undergoes an unconventional two-dome evolution in the critical temperature, which suggests a complex intertwinement of the CDW state and superconductivity [32,33]. At present, the microscopic interacting mechanism underlying the above correlated states is challenging, and remains elusive [34–37]. First, it is helpful to know the correspondence between simple forms of interactions and their induced symmetry-breaking orders on a kagome lattice. Nevertheless, up to now, the prototype models of interacting fermions on a kagome lattice are still less investigated than their counterparts on square and honeycomb geometries [38–47].

In this paper, we perform a systematic study of an attractive kagome-lattice Hubbard model, with the aim of estimating the relevance of attractive on-site interactions to the experimental

*hmguo@buaa.edu.cn

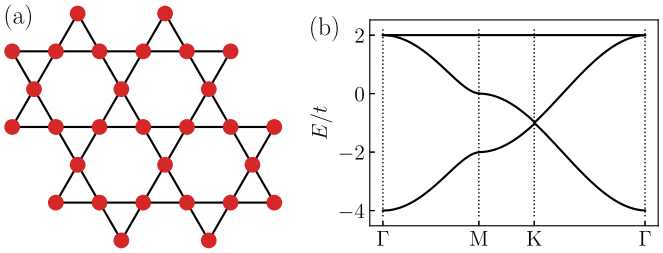

FIG. 1. (a) The geometry of the kagome lattice, which is a triangular Bravais lattice with a three-site unit cell. (b) The band structure along the high-symmetry directions in the Brillouin zone.

discoveries. We first analyze the physical property of possible CDW orders at $\rho = 2/3$, and perform a mean-field study of the CDW phase transition. Then determinant quantum Monte Carlo (DQMC) is applied to unveil the correlated phases therein. From the charge correlation function, an instability to CDW patterns is found, satisfying that the triangle rule may occur at the Dirac points. Next, we calculate the s-wave pair structure factor, and map out the phase diagrams in the (μ, T) plane. Although the finite-size effect is apparent in small lattices, robust superconducting domes exist for large values of U, L. Finally, we determine the superconducting (SC) transition temperature using finite-size scaling. These results suggest that the s-wave superconductivity supported by some experiments in AV_3Sb_5 may originate from an electronic attractive on-site interaction.

This paper is organized as follows. Section II introduces the model we will investigate, along with our computational methodology. Section III presents the mean-field theory for the CDW transition. Section IV uses DQMC simulations to study a possible CDW state at 1/3 filling and superconductivity with on-site pairing. Section VI gives the conclusions.

II. MODEL AND METHOD

We start from the attractive kagome-lattice Hubbard model,

$$H = -t \sum_{\langle ij\rangle\sigma} c^\dagger_{i\sigma} c_{j\sigma} - U \sum_i \left(n_{i\uparrow} - \frac{1}{2}\right)\left(n_{i\downarrow} - \frac{1}{2}\right), \quad (1)$$

where $c^\dagger_{i\sigma}$ and $c_{i\sigma}$ are the creation and annihilation operators, respectively, at site i with spin $\sigma = \uparrow, \downarrow$; $\langle ij\rangle$ denotes nearest neighbors; $n_{i\sigma} = c^\dagger_{i\sigma} c_{i\sigma}$ is the number of electrons of spin σ on site i, and U is the on-site attractive interaction. Throughout the paper, the hopping amplitude is set to $t = 1$ as the unit of energy.

The kagome lattice has a three-site unit cell [Fig. 1(a)]. In momentum space, the $U = 0$ Hamiltonian is given by [8]

$$\mathcal{H}_0(\mathbf{k}) = -2t \begin{pmatrix} 0 & \cos k_1 & \cos k_3 \\ \cos k_1 & 0 & \cos k_2 \\ \cos k_3 & \cos k_2 & 0 \end{pmatrix}, \quad (2)$$

where $k_n = \mathbf{k} \cdot \mathbf{a}_n$ (the sublattice index $n = 1, 2, 3$) with $\mathbf{a}_1 = (1, 0)$, $\mathbf{a}_2 = (-1, \sqrt{3})/2$, and $\mathbf{a}_3 = -(\mathbf{a}_1 + \mathbf{a}_2)$. The spectrum of $\mathcal{H}_0(\mathbf{k})$ has one flat band $E_3(\mathbf{k}) = 2t$ and two dispersive ones,

$$E_{1,2}(\mathbf{k}) = t[-1 \pm \sqrt{4f(\mathbf{k}) - 3}], \quad (3)$$

with $f(\mathbf{k}) = \cos^2 k_1 + \cos^2 k_2 + \cos^2 k_3$. Bands 1 and 2 touch at two inequivalent Dirac points $\mathbf{K}_\pm = (\pm 2\pi/3, 0)$ at energy $-t$ [see Fig. 1(b)]. For 1/3 filling, the lowest band is filled, and the low-energy excitations resemble those of graphene, which are linear, $\epsilon_{1,2} = \pm\sqrt{3}t|\vec{q}|$, with $\vec{q} = (q_x, q_y)$ a small displacement away from the Dirac points.

At finite interactions, Eq. (1) is solved numerically via DQMC, where one decouples the on-site interaction term through the introduction of an auxiliary Hubbard-Stratonovich field, which is integrated out stochastically. The only errors are those associated with the statistical sampling, the finite spatial lattice size, and the inverse temperature discretization. These errors are well controlled in the sense that they can be systematically reduced as needed, and further eliminated by appropriate extrapolations. Unlike the repulsive Hubbard model on a kagome lattice where the infamous sign problem exists at all densities [48–50], the attractive case under our investigation is free of the sign problem [51–55]. This allows DQMC to reach the low temperatures needed to study the ground-state properties. In the following, we use the inverse temperature discretization $\Delta\tau = 1/16$, and the lattice has $N = 3 \times L \times L$ sites with L up to 12.

III. MEAN-FIELD THEORY

To explore possible CDW orders at $\rho = 2/3$, we first investigate the physical properties of the CDW order preserving the translation symmetry of the kagome lattice. The following CDW term is added to the noninteracting Hamiltonian in Eq. (2),

$$\mathcal{H}_{\mathrm{CDW}}(\mathbf{k}) = \mathrm{diag}(w_1, w_2, w_3), \quad (4)$$

where w_l ($l = 1, 2, 3$) represents the on-site potential of the lth sublattice. Since it is independent of spin, we can discard the spin index, and focus on the spinless case at $\rho = 1/3$.

Here, a central concern is whether the above CDW can open up a gap at the Dirac points. This is more easily revealed based on the low-energy Hamiltonian, which can be obtained by linearizing $\mathcal{H}_\mathbf{k} = \mathcal{H}_0(\mathbf{k}) + \mathcal{H}_{\mathrm{CDW}}(\mathbf{k})$ near $\mathbf{K}_\pm$ and subsequently projecting onto the subspace associated with the two lowest bands. With the above procedure, we find the following low-energy Hamiltonian,

$$h_\ell(\mathbf{k}) = v\left[\sigma_z\left(k_x - \mathcal{A}^\ell_x\right) + \sigma_x\left(k_y - \mathcal{A}^\ell_y\right)\right] + \mathbb{1}w \quad (5)$$

for valley ℓ, with the Fermi velocity $v = \sqrt{3}t$, $w = (w_1 + w_2 + w_3)/3$, and

$$\mathcal{A}^\ell_x = (2w_2 - w_1 - w_3)\ell/6v,$$
$$\mathcal{A}^\ell_y = (w_1 - w_3)\ell/6t.$$

Thus the CDW couples to the Dirac fermions as a gauge field, which moves the positions of the Dirac point in the Brillouin zone, and does not open up a gap. Nevertheless, when the CDW is large enough to make the two Dirac points meet and merge with each other, the system becomes gapped. This is in great contrast to the situation in graphene, where an on-site staggered potential always opens up a gap at the Dirac points.

Then it is helpful to perform a mean-field (MF) analysis of the Hamiltonian Eq. (2) to reveal possible CDW orders. In

the MF approximation, the interaction term in Eq. (2) can be decoupled as

$$n_{i,\uparrow}n_{i,\downarrow} = \langle n_{i,\uparrow}\rangle n_{i,\downarrow} + n_{i,\uparrow}\langle n_{i,\downarrow}\rangle - \langle n_{i,\uparrow}\rangle\langle n_{i,\downarrow}\rangle. \quad (6)$$

To perform a mean-field decomposition, one needs to preliminarily assume the configuration of the charge order. There may be various kinds of CDW phases at the low filling $\rho = 2/3$. To get some clues, let us first recall the situation in the bipartite square and honeycomb lattices. At half filling, the attractive model can be exactly mapped on a repulsive one by the following transformation, $c_{j\uparrow} \to \bar{c}_{j\uparrow}$ and $c_{j\downarrow} \to \bar{c}^{\dagger}_{j\downarrow} = (-1)^j c_{j\downarrow}$, where j is even (odd) on one (the other) sublattice. The z (xy) component of the SU(2) symmetric antiferromagnetism in the repulsive model corresponds to the CDW (superconducting) phase in the attractive one. Specifically, the CDW is composed of alternating empty and doubly occupied sites. The above knowledge gives us the following implication for the attractive kagome-lattice model: The doubly occupied sites are favored by negative U; the electron-rich sites tend to be far away from each other. Hence we consider a set of well-established CDWs in the literature satisfying the triangle rule [15]: Each unit cell of a kagome lattice only contains one electron-rich site, and it is always surrounded by electron-poor sites at the nearest neighbors. There are still multiple such CDWs, and herein we focus on a simple configuration in which one specific sublattice is occupied by majority electrons. To incorporate the above CDW order, the average of the number operator is written as $\langle n_{i,\sigma}\rangle = \rho_l$ with ρ_l the order parameter. Since the assumed CDW preserves the translation symmetry of the kagome lattice, ρ_l may only differ within the unit cell, and takes three values ρ_l ($l = 1, 2, 3$). Then the attractive Hubbard interaction becomes

$$-U\sum_i n_{i,\uparrow}n_{i,\downarrow} = -U\sum_{l=1,2,3}\sum_{i\in l}\rho_l n_i + E_0, \quad (7)$$

where $n_i = n_{i,\uparrow} + n_{i,\downarrow}$ is the operator of total number of electrons, and $E_0 = \frac{NU}{3}(\rho_1^2 + \rho_2^2 + \rho_3^2)$ with N the total number of sites is a constant. In the momentum space, the MF Hamiltonian is written as

$$\mathcal{H}^{\sigma}_{\mathrm{MF}}(\mathbf{k}) = \mathcal{H}^{\sigma}_0(\mathbf{k}) + \mathcal{H}_{\mathrm{diag}}, \quad (8)$$

with

$$\mathcal{H}_{\mathrm{diag}} = \begin{pmatrix} -U\rho_1 & 0 & 0 \\ 0 & -U\rho_2 & 0 \\ 0 & 0 & -U\rho_3 \end{pmatrix}. \quad (9)$$

The energy spectrum is directly obtained by diagonalizing the above Hamiltonian. Supposing the low-energy band is E_k (degenerate for both spin copies), the total ground-state energy is $E_{\mathrm{tot}} = 2\sum_{\mathbf{k}} E_{\mathbf{k}} + E_0$. Minimizing E_{tot} with respect to ρ_l, we can obtain the self-consistent equation for the order parameters

$$\rho_l = -\frac{3}{2UN}\frac{\partial E_{\mathrm{tot}}}{\partial \rho_l}. \quad (10)$$

Figure 2 plots the order parameters ρ_l calculated self-consistently as a function of U. The order parameter is uniform, and all equal to 1/3 at small interactions. Then at a critical strength $U_c/t = 4.54$, the curves suddenly split into two branches, and the value of ρ_1 becomes much larger than that of ρ_2, ρ_3 ($\rho_2 = \rho_3$), suggesting the occurrence of a CDW phase transition.

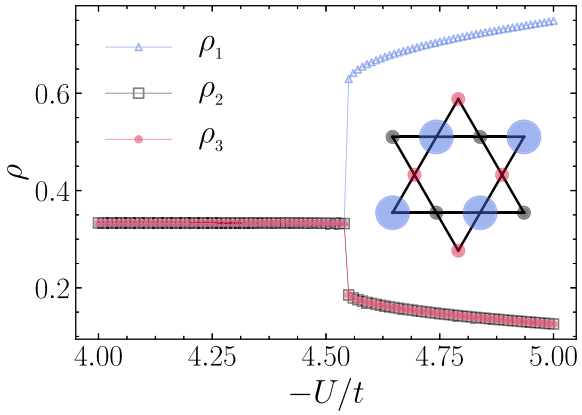

FIG. 2. The mean-field order parameters ρ_1, ρ_2, and ρ_3 as a function of U. The curves exhibit a discontinuity marking the CDW phase transition, and the critical interaction is determined to be $U_c/t = -4.54$.

IV. DQMC RESULTS

A. CDW at 1/3 filling

Next, we apply DQMC to unveil the physical properties of the Hamiltonian in Eq. (1) quantitatively. Figure 3 plots the average density $\rho = \frac{1}{N}\sum_{i\sigma}\langle n_{i\sigma}\rangle$ vs μ for various values of U. There exist evident finite-size plateaus near the Dirac density $\rho = 2/3$, which persist up to $U/t \sim -4$. Afterwards, ρ continuously increases with μ, and the curves show no special features. As discussed above, since the CDW may not gap out the Dirac points, it is unclear here whether a $\rho = 2/3$ CDW has been induced by large attractive interactions.

In order to detect the possible CDW phase, we plot in Fig. 4 the real-space charge-charge correlation function, which is defined as $C(\mathbf{r}) = \langle n_i n_{i+\mathbf{r}}\rangle$ with $n_i = n_{i\uparrow} + n_{i\downarrow}$. $C(\mathbf{r})$ is nearly uniform over the whole lattice except the nearest-neighbor (NN) charge correlations, whose values are apparently smaller than the other ones. We further calculate the ratio $R = C(\mathbf{r}_{\mathrm{nn}})/C(\mathbf{r}_{\mathrm{max}})$ with $\mathbf{r}_{\mathrm{nn}}$ ($\mathbf{r}_{\mathrm{max}}$) the NN (maximum) distance in the lattice. It is found that as the average density increases and goes away from $\rho = 2/3$, R increases continuously, and

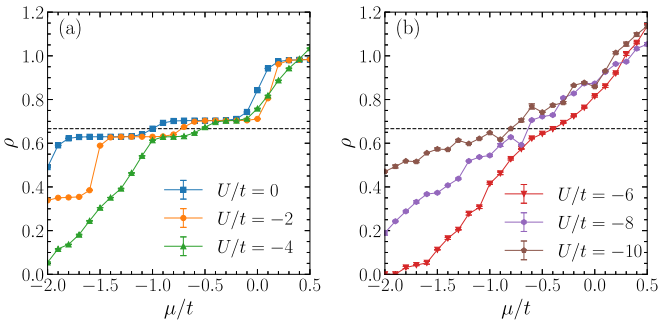

FIG. 3. The average density as a functions of μ at the attractive interaction (a) $U/t = 0, -2, -4$ and (b) $U/t = -6, -8, -10$. Here, the lattice size is $L = 6$, and the inverse temperature is $\beta t = 18$.

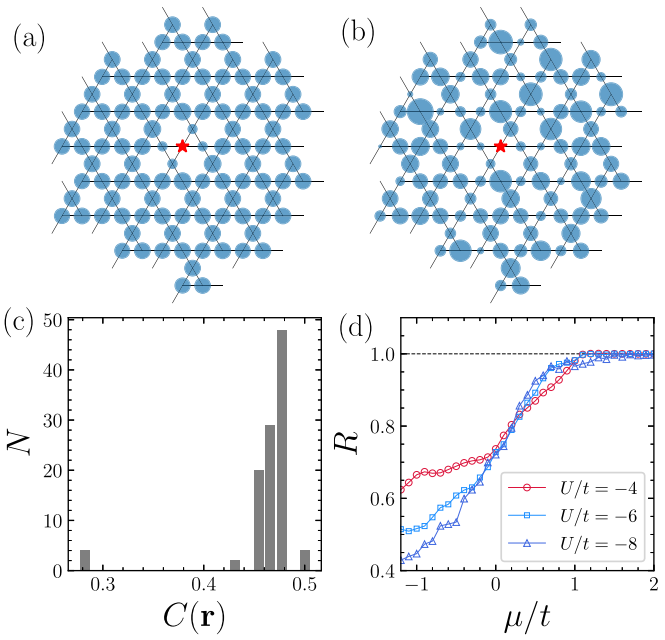

FIG. 4. (a) The charge correlation function $C(\mathbf{r})$ for $\mu/t = -0.4$ (corresponding to $\rho = 2/3$) on an $L = 6$ lattice. The red star marks the reference site, and the magnitude of the correlation is represented by the radii of the solid blue circle. (b) $C(\mathbf{r})$ in one updated configuration of the DQMC measurement of (a). (c) The distribution of the values of $C(\mathbf{r})$ in (a). (d) The ratio $R = C(\mathbf{r}_{\rm nn})/C(\mathbf{r}_{\rm max})$ as a function of chemical potential. Here, the interaction strength in (a)–(c) is $U/t = -8$. The inverse temperature $\beta t = 12$ is used in all panels.

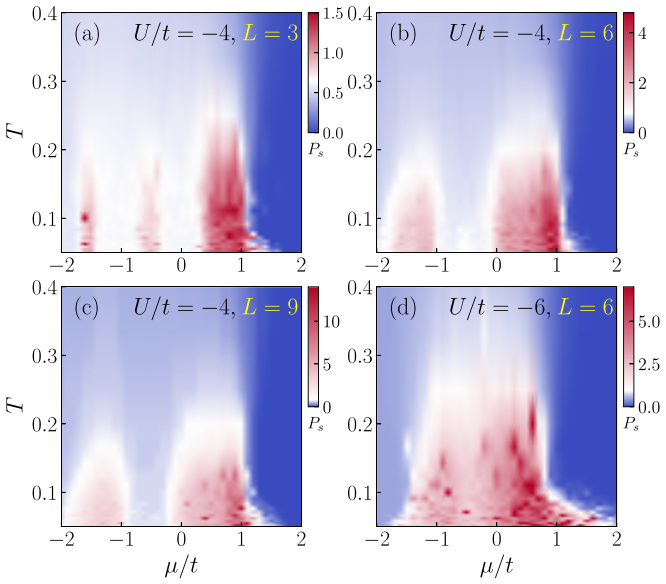

FIG. 5. The pair structure factor P_s in the space of parameters T/t vs μ/t at $U/t = -4$ for lattice sizes (a) $L = 3$, (b) $L = 6$, and (c) $L = 9$. (d) Similar plot with $U/t = -6$ and $L = 6$.

becomes uniform from $\mu/t \sim 1$. Although no CDW pattern is identified at $\rho = 2/3$, each configuration in the histogram of DQMC measurements has clearly inhomogeneous charge correlations. The above behavior may be due to the multifold degeneracy of the CDW phase fulfilling the triangle rule. After averaging over the different charge patterns, the charge correlations become uniform. Nevertheless, since the triangle rule always restricts the occupation of the NN sites in all degenerate configurations, the value of the NN charge correlations remains greatly reduced. Hence, our results provide indirect evidence for the existence of CDW patterns satisfying the triangle rule.

B. Superconductivity with on-site pairing

The s-wave superconductivity is characterized by the pair structure factor,

$$P_s = \langle \Delta^\dagger \Delta + \Delta \Delta^\dagger \rangle, \tag{11}$$

with

$$\Delta^\dagger = \frac{1}{\sqrt{N}} \sum_i c^\dagger_{i\uparrow} c^\dagger_{i\downarrow}. \tag{12}$$

Figure 5 plots the pair structure factor in the (μ, T) plane for several lattice sizes. For a small lattice, the finite-size effect is very apparent, which is similar to what has been observed in the attractive Hubbard model on the square lattice [56]. As shown in Fig. 5(a), the s-wave pairing is enhanced at sufficiently low temperatures near several special values of μ/t. This behavior has been attributed to the coarse discretization of the Brillouin zone in small lattices, which persists even at a moderate interaction $U/t = -4$. As the lattice size increases, there remain two disconnected superconducting domes. As shown in Figs. 5(b) and 5(c), the gap between them decreases with lattice size, and seems highly related to the flat region of the average density near $\rho = 2/3$. For a stronger interaction strength $U/t = -6$, there is only one large superconducting dome in the phase diagram. Correspondingly, there are no visible plateaus in the curve of the average density.

Next, we perform a quantitative analysis of the superconducting critical temperature. Here, we focus on a density of $\rho = 1.35$ instead of the case of the Dirac filling $\rho = 2/3$ associated with a CDW phase. The reason is that the finite-size effect is very severe at $\rho = 2/3$, and it is difficult to perform a proper finite-size scaling. As shown in Fig. 5, s-wave superconductivity exists at nearly all fillings. So to obtain a quantitative analysis of the critical temperature, we take $\mu/t = 0.9$ (corresponding to $\rho = 1.35$), where the superconductivity is most predominant for $U/t = -4$, allowing a reasonable finite-size scaling with relatively small lattice sizes. As the temperature is lowered, the pair structure factor increases monotonically [see Fig. 6(a)]. For high temperatures, P_s is size independent due to the absence of superconducting long-range order. Conversely, P_s increases significantly with the lattice size at low temperatures, which is a hallmark of the occurrence of the superconducting state. The usual way to investigate the properties of the Hubbard model is to fix the average density. However, since DQMC works in a grand-canonical ensemble, the above routine has an increased overhead to determine the chemical potential that produces the desired filling. Here, we choose to fix the chemical potential for different temperatures. In the temperature range of interest

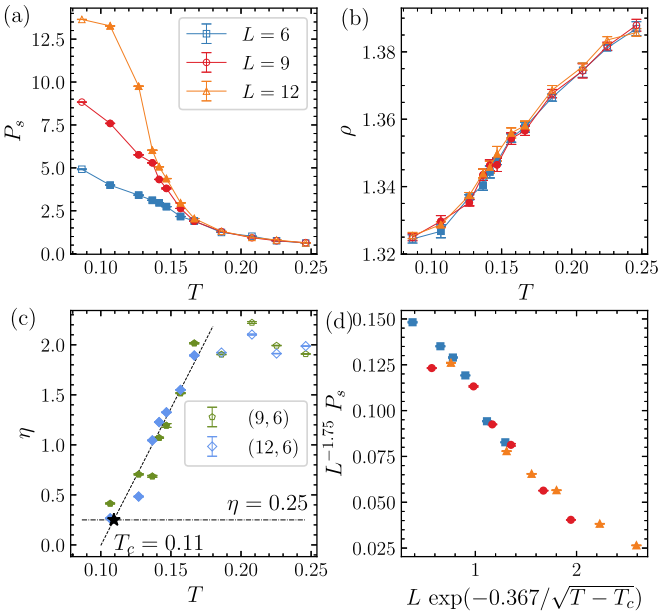

FIG. 6. (a) P_s as a function of temperature T for various lattice sizes. (b) The average density vs T, which correspond to the plots in (a). (c) The exponent $\eta(T)$ extracted according to Eq. (15) as a function of temperature. The critical temperature is determined to be $T_c = 0.11$ by the condition $\eta(T_c) = 0.25$. (d) The collapse of the curves in (a) using the scaling form Eq. (14) and T_c determined in (c). The data points shown as solid circles in (a) and (b) are above T_c, and are used for the extraction and scaling in (c) and (d). (L', L) in the legend of (c) represents the two different lattice sizes in Eq. (15), with L the reference one. Here, $A = -0.367$ is used to obtain the best collapse. The interaction strength $U/t = -4$ and the chemical potential $\mu/t = 0.9$ are used.

$(T/t = 0.1$–$0.16)$, this routine results in a slight deviation of the densities around $\rho = 1.35$ [see Fig. 6(b)].

One expects the decay of the real-space correlations as follows,

$$C(r) \equiv \langle c^\dagger_{\mathbf{i}\uparrow} c^\dagger_{\mathbf{i}\downarrow} c_{\mathbf{j}\downarrow} c_{\mathbf{j}\uparrow} + \text{H.c.} \rangle \sim r^{-\eta(T)}, \tag{13}$$

where $r = |\mathbf{i} - \mathbf{j}|$. Then the pair structure factor scales as

$$P_s = L^{2-\eta(T)} f(L/\xi), \tag{14}$$

with the coherence length $\xi \sim \exp[-A/(T - T_c)^{\frac{1}{2}}]$ [51,52,55,56]. Here, $\eta(T)$ is temperature dependent, and can be extracted by dividing the above scaling form from two different lattice sizes L, L'. The obtained exponent is written as

$$\eta(T) = 2 - \frac{\ln [P_s(L, T)/P_s(L', T)]}{\ln (L/L')}. \tag{15}$$

We take an $L = 6$ lattice as the reference one, and the extracted $\eta(T)$ at each temperature according to the above equation is illustrated in Fig. 6(c). At high temperatures, the pair structure factor has a negligible size dependence, thus the exponent $\eta(T)$ saturates around 2 in this regime. Otherwise, in the $T \to T_c$ limit, $\eta(T_c) = 0.25$ is expected. Above T_c, $\eta(T)$ increases monotonically to the saturated value 2. By a linear fit of the increasing regime, the critical temperature is determined to be $T_c/t = 0.11$ for $U/t = -4$ and $\mu/t = 0.9$. Subsequently, we collapse P_s of different lattice sizes using the scaling form in Eq. (14) with the above T_c and A being adjusted to give the best data collapse. As shown in Fig. 6(d), the collapse onto a single curve is rather good for the $\eta(T)$-increasing region.

V. CONCLUSIONS

We investigate the attractive kagome-lattice Hubbard model with two complementary methods: the mean-field theory and large-scale DQMC simulations. The mean-field analysis predicts a CDW transition, with the configuration of the CDW order satisfying the triangle rule. Subsequent DQMC simulations provide indirect evidence for its existence at strong interactions. Then, by calculating the pair structure factor, s-wave superconductivity is shown to be stabilized at low temperatures, and exists in dome regions of the phase diagrams. We finally determine the superconducting critical

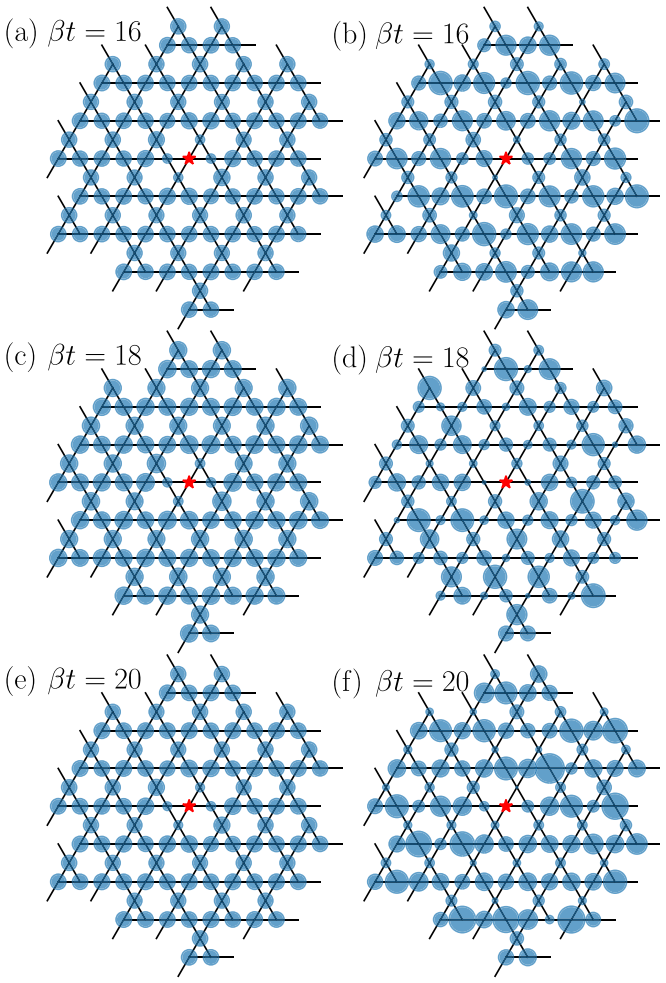

FIG. 7. The charge correlation function $C(\mathbf{r})$ at $\rho = 2/3$ on an $L = 6$ lattice: (a) $\beta t = 16$ and $\mu/t = -0.5$; (c) $\beta t = 18$ and $\mu/t = -0.8$; (e) $\beta t = 20$ and $\mu/t = -0.7$. (b), (d), and (f) are $C(\mathbf{r})$ in one updated configuration of the DQMC measurements of (a), (c), and (e), respectively. The red star marks the reference site, and the magnitude of the correlation is represented by the radii of the solid blue circle. The chemical potential corresponding to $\rho = 2/3$ varies with temperature. Here, the interaction strength is $U/t = -8$.

temperature quantitatively by finite-size scaling of the pair structure factor.

The pairing symmetry is important to understand the SC mechanism in AV_3Sb_5. Its two aspects, i.e., a gap structure and the nature of the spin pairing state, have been much investigated experimentally. Unexpectedly, various techniques have yielded inconsistent results, including singlet or triplet spin pairing, and nodeless or node gap functions [57–62]. The complexity may be due to the multiband nature of the SC state, and it is still challenging to reconcile the apparently contradictory observations. Nevertheless, our results suggest an s-wave pairing mechanism by the attractive Hubbard interaction, which may be helpful in understanding the complex SC phenomena in kagome materials.

ACKNOWLEDGMENTS

The authors thank Fan Yang and Wen Yang for helpful discussions. H.G. acknowledge support from the National Natural Science Foundation of China (NSFC) Grants No. 11774019 and No. 12074022, and the NSAF grant in NSFC with Grant No. U1930402. S.F. is supported by the National Key Research and Development Program of China under Grant No. 2021YFA1401803, and NSFC under Grants No. 11974051 and No. 12274036. X.Z. is supported by the Fundamental Research Funds for the Central Universities (Grant No. AE89991/383).

APPENDIX: CHARGE CORRELATION FUNCTIONS AT LOWER TEMPERATURES

In Fig. 4 of the main text, we show the charge correlation function at $\beta t = 12$ for $\rho = 2/3$ and $U/t = -8$. To address the effect of thermal fluctuation, we have carried out DQMC simulations at lower temperatures, and find the results are similar (see Fig. 7). Thus the inverse temperature $\beta t = 12$ is large enough to produce the properties of the ground state.

[1] M. Mekata, Kagome: The story of the basketweave lattice, Phys. Today **56**(2), 12 (2003).
[2] L. Balents, Spin liquids in frustrated magnets, Nature (London) **464**, 199 (2010).
[3] S. Yan, D. A. Huse, and S. R. White, Spin-liquid ground state of the $s = 1/2$ kagome Heisenberg antiferromagnet, Science **332**, 1173 (2011).
[4] L. Savary and L. Balents, Quantum spin liquids: A review, Rep. Prog. Phys. **80**, 016502 (2017).
[5] Y. Zhou, K. Kanoda, and T.-K. Ng, Quantum spin liquid states, Rev. Mod. Phys. **89**, 025003 (2017).
[6] C. Broholm, R. J. Cava, S. A. Kivelson, D. G. Nocera, M. R. Norman, and T. Senthil, Quantum spin liquids, Science **367**, eaay0668 (2020).
[7] M. R. Norman, Colloquium: Herbertsmithite and the search for the quantum spin liquid, Rev. Mod. Phys. **88**, 041002 (2016).
[8] H.-M. Guo and M. Franz, Topological insulator on the kagome lattice, Phys. Rev. B **80**, 113102 (2009).
[9] L. Ye, M. Kang, J. Liu, F. Von Cube, C. R. Wicker, T. Suzuki, C. Jozwiak, A. Bostwick, E. Rotenberg, D. C. Bell *et al.*, Massive Dirac fermions in a ferromagnetic kagome metal, Nature (London) **555**, 638 (2018).
[10] E. Liu, Y. Sun, N. Kumar, L. Muechler, A. Sun, L. Jiao, S.-Y. Yang, D. Liu, A. Liang, Q. Xu *et al.*, Giant anomalous Hall effect in a ferromagnetic kagome-lattice semimetal, Nat. Phys. **14**, 1125 (2018).
[11] J.-X. Yin, S. S. Zhang, H. Li, K. Jiang, G. Chang, B. Zhang, B. Lian, C. Xiang, I. Belopolski, H. Zheng *et al.*, Giant and anisotropic many-body spin–orbit tunability in a strongly correlated kagome magnet, Nature (London) **562**, 91 (2018).
[12] Z. Lin, J.-H. Choi, Q. Zhang, W. Qin, S. Yi, P. Wang, L. Li, Y. Wang, H. Zhang, Z. Sun, L. Wei, S. Zhang, T. Guo, Q. Lu, J.-H. Cho, C. Zeng, and Z. Zhang, Flatbands and Emergent Ferromagnetic Ordering in Fe_3Sn_2 Kagome Lattices, Phys. Rev. Lett. **121**, 096401 (2018).
[13] M. Kang, L. Ye, S. Fang, J.-S. You, A. Levitan, M. Han, J. I. Facio, C. Jozwiak, A. Bostwick, E. Rotenberg *et al.*, Dirac fermions and flat bands in the ideal kagome metal FeSn, Nat. Mater. **19**, 163 (2020).
[14] A. O'Brien, F. Pollmann, and P. Fulde, Strongly correlated fermions on a kagome lattice, Phys. Rev. B **81**, 235115 (2010).
[15] J. Wen, A. Rüegg, C.-C. J. Wang, and G. A. Fiete, Interaction-driven topological insulators on the kagome and the decorated honeycomb lattices, Phys. Rev. B **82**, 075125 (2010).
[16] F. Pollmann, K. Roychowdhury, C. Hotta, and K. Penc, Interplay of charge and spin fluctuations of strongly interacting electrons on the kagome lattice, Phys. Rev. B **90**, 035118 (2014).
[17] M. L. Kiesel, C. Platt, and R. Thomale, Unconventional Fermi Surface Instabilities in the Kagome Hubbard Model, Phys. Rev. Lett. **110**, 126405 (2013).
[18] S.-L. Yu and J.-X. Li, Chiral superconducting phase and chiral spin-density-wave phase in a Hubbard model on the kagome lattice, Phys. Rev. B **85**, 144402 (2012).
[19] M. L. Kiesel and R. Thomale, Sublattice interference in the kagome Hubbard model, Phys. Rev. B **86**, 121105(R) (2012).
[20] W.-S. Wang, Z.-Z. Li, Y.-Y. Xiang, and Q.-H. Wang, Competing electronic orders on kagome lattices at van Hove filling, Phys. Rev. B **87**, 115135 (2013).
[21] W.-S. Wang, Y.-C. Liu, Y.-Y. Xiang, and Q.-H. Wang, Antiferromagnetism, f-wave, and chiral p-wave superconductivity in a kagome lattice with possible application to sd^2 graphenes, Phys. Rev. B **94**, 014508 (2016).
[22] B. R. Ortiz, L. C. Gomes, J. R. Morey, M. Winiarski, M. Bordelon, J. S. Mangum, I. W. H. Oswald, J. A. Rodriguez-Rivera, J. R. Neilson, S. D. Wilson, E. Ertekin, T. M. McQueen, and E. S. Toberer, New kagome prototype materials: Discovery of KV_3Sb_5, RbV_3Sb_5, and CsV_3Sb_5, Phys. Rev. Mater. **3**, 094407 (2019).
[23] K. Jiang, T. Wu, J.-X. Yin, Z. Wang, M. Z. Hasan, S. D. Wilson, X. Chen, and J. Hu, Kagome superconductors AV_3Sb_5 (A= K, Rb, Cs), Natl. Sci. Rev. **10**, nwac199 (2023).

[24] T. Nguyen and M. Li, Electronic properties of correlated kagomé metals AV_3Sb_5 (A = K, Rb, and Cs): A perspective, J. Appl. Phys. **131**, 060901 (2022).

[25] T. Neupert, M. M. Denner, J.-X. Yin, R. Thomale, and M. Z. Hasan, Charge order and superconductivity in kagome materials, Nat. Phys. **18**, 137 (2022).

[26] H. Zhao, H. Li, B. R. Ortiz, S. M. L. Teicher, T. Park, M. Ye, Z. Wang, L. Balents, S. D. Wilson, and I. Zeljkovic, Cascade of correlated electron states in the kagome superconductor CsV_3Sb_5, Nature (London) **599**, 216 (2021).

[27] M. Kang, S. Fang, J.-K. Kim, B. R. Ortiz, S. H. Ryu, J. Kim, J. Yoo, G. Sangiovanni, D. Di Sante, B.-G. Park *et al.*, Twofold van Hove singularity and origin of charge order in topological kagome superconductor CsV_3Sb_5, Nat. Phys. **18**, 301 (2022).

[28] Y.-X. Jiang, J.-X. Yin, M. M. Denner, N. Shumiya, B. R. Ortiz, G. Xu, Z. Guguchia, J. He, M. S. Hossain, X. Liu *et al.*, Unconventional chiral charge order in kagome superconductor KV_3Sb_5, Nat. Mater. **20**, 1353 (2021).

[29] X. Feng, K. Jiang, Z. Wang, and J. Hu, Chiral flux phase in the kagome superconductor AV_3Sb_5, Sci. Bull. **66**, 1384 (2021).

[30] C. Mielke, D. Das, J.-X. Yin, H. Liu, R. Gupta, Y.-X. Jiang, M. Medarde, X. Wu, H. Lei, J. Chang *et al.*, Time-reversal symmetry-breaking charge order in a kagome superconductor, Nature (London) **602**, 245 (2022).

[31] L. Nie, K. Sun, W. Ma, D. Song, L. Zheng, Z. Liang, P. Wu, F. Yu, J. Li, M. Shan *et al.*, Charge-density-wave-driven electronic nematicity in a kagome superconductor, Nature (London) **604**, 59 (2022).

[32] K. Y. Chen, N. N. Wang, Q. W. Yin, Y. H. Gu, K. Jiang, Z. J. Tu, C. S. Gong, Y. Uwatoko, J. P. Sun, H. C. Lei, J. P. Hu, and J.-G. Cheng, Double Superconducting Dome and Triple Enhancement of T_c in the Kagome Superconductor CsV_3Sb_5 under High Pressure, Phys. Rev. Lett. **126**, 247001 (2021).

[33] F. H. Yu, D. H. Ma, W. Z. Zhuo, S. Q. Liu, X. K. Wen, B. Lei, J. J. Ying, and X. H. Chen, Unusual competition of superconductivity and charge-density-wave state in a compressed topological kagome metal, Nat. Commun. **12**, 1 (2021).

[34] X. Wu, T. Schwemmer, T. Müller, A. Consiglio, G. Sangiovanni, D. Di Sante, Y. Iqbal, W. Hanke, A. P. Schnyder, M. M. Denner, M. H. Fischer, T. Neupert, and R. Thomale, Nature of Unconventional Pairing in the Kagome Superconductors AV_3Sb_5 (A = K, Rb, Cs), Phys. Rev. Lett. **127**, 177001 (2021).

[35] H. Tan, Y. Liu, Z. Wang, and B. Yan, Charge Density Waves and Electronic Properties of Superconducting Kagome Metals, Phys. Rev. Lett. **127**, 046401 (2021).

[36] J. Zhao, W. Wu, Y. Wang, and S. A. Yang, Electronic correlations in the normal state of the kagome superconductor KV_3Sb_5, Phys. Rev. B **103**, L241117 (2021).

[37] H. D. Scammell, J. Ingham, T. Li, and O. P. Sushkov, Chiral excitonic order from twofold van Hove singularities in kagome metals, Nat. Commun. **14**, 605 (2023).

[38] Z. Y. Meng, T. C. Lang, S Wessel, F. F. Assaad, and A. Muramatsu, Quantum spin liquid emerging in two-dimensional correlated Dirac fermions, Nature (London) **464**, 847 (2010).

[39] S. Sorella, Y. Otsuka, and S. Yunoki, Absence of a spin liquid phase in the Hubbard model on the honeycomb lattice, Sci. Rep. **2**, 992 (2012).

[40] F. F. Assaad and I. F. Herbut, Pinning the Order: The Nature of Quantum Criticality in the Hubbard Model on Honeycomb Lattice, Phys. Rev. X **3**, 031010 (2013).

[41] Y. Otsuka, S. Yunoki, and S. Sorella, Universal Quantum Criticality in the Metal-Insulator Transition of Two-Dimensional Interacting Dirac Electrons, Phys. Rev. X **6**, 011029 (2016).

[42] T. Paiva, R. T. Scalettar, W. Zheng, R. R. P. Singh, and J. Oitmaa, Ground-state and finite-temperature signatures of quantum phase transitions in the half-filled Hubbard model on a honeycomb lattice, Phys. Rev. B **72**, 085123 (2005).

[43] F. Parisen Toldin, M. Hohenadler, F. F. Assaad, and I. F. Herbut, Fermionic quantum criticality in honeycomb and π-flux Hubbard models: Finite-size scaling of renormalization-group-invariant observables from quantum Monte Carlo, Phys. Rev. B **91**, 165108 (2015).

[44] C. Wen, X. Zhu, Z. Xiao, N. Hao, R. Mondaini, H. Guo, and S. Feng, Superconducting pairing symmetry in the kagome-lattice Hubbard model, Phys. Rev. B **105**, 075118 (2022).

[45] C. Wen, X. Zhu, N. Hao, H. Guo, and S. Feng, Unconventional ferromagnetism and spin-triplet superconductivity in the imbalanced kagome-lattice Hubbard model, Phys. Rev. B **105**, 245131 (2022).

[46] R.-Y. Sun and Z. Zhu, Metal-insulator transition and intermediate phases in the kagome lattice Hubbard model, Phys. Rev. B **104**, L121118 (2021).

[47] J. Kaufmann, K. Steiner, R. T. Scalettar, K. Held, and O. Janson, How correlations change the magnetic structure factor of the kagome Hubbard model, Phys. Rev. B **104**, 165127 (2021).

[48] E. Y. Loh, J. E. Gubernatis, R. T. Scalettar, S. R. White, D. J. Scalapino, and R. L. Sugar, Sign problem in the numerical simulation of many-electron systems, Phys. Rev. B **41**, 9301 (1990).

[49] M. Troyer and U.-J. Wiese, Computational Complexity and Fundamental Limitations to Fermionic Quantum Monte Carlo Simulations, Phys. Rev. Lett. **94**, 170201 (2005).

[50] V. I. Iglovikov, E. Khatami, and R. T. Scalettar, Geometry dependence of the sign problem in quantum Monte Carlo simulations, Phys. Rev. B **92**, 045110 (2015).

[51] A. Moreo and D. J. Scalapino, Two-Dimensional Negative-U Hubbard Model, Phys. Rev. Lett. **66**, 946 (1991).

[52] R. T. Scalettar, E. Y. Loh, J. E. Gubernatis, A. Moreo, S. R. White, D. J. Scalapino, R. L. Sugar, and E. Dagotto, Phase Diagram of the Two-Dimensional Negative-U Hubbard Model, Phys. Rev. Lett. **62**, 1407 (1989).

[53] R. R. dos Santos, Attractive Hubbard model on a triangular lattice, Phys. Rev. B **48**, 3976 (1993).

[54] K. L. Lee, K. Bouadim, G. G. Batrouni, F. Hébert, R. T. Scalettar, C. Miniatura, and B. Grémaud, Attractive Hubbard model on a honeycomb lattice: Quantum Monte Carlo study, Phys. Rev. B **80**, 245118 (2009).

[55] T. Paiva, R. R. dos Santos, R. T. Scalettar, and P. J. H. Denteneer, Critical temperature for the two-dimensional attractive Hubbard model, Phys. Rev. B **69**, 184501 (2004).

[56] R. Mondaini, S. Tarat, and R. T. Scalettar, Universality and critical exponents of the fermion sign problem, arXiv:2207.09026.

[57] C. Mu, Q. Yin, Z. Tu, C. Gong, H. Lei, Z. Li, and J. Luo, S-wave superconductivity in kagome metal CsV_3Sb_5 revealed by $^{121/123}$Sb NQR and ^{51}V NMR measurements, Chin. Phys. Lett. **38**, 077402 (2021).

[58] S. Ni, S. Ma, Y. Zhang, J. Yuan, H. Yang, Z. Lu, N. Wang, J. Sun, Z. Zhao, D. Li *et al.*, Anisotropic superconducting prop-

erties of kagome metal CsV_3Sb_5, Chin. Phys. Lett. **38**, 057403 (2021).

[59] H.-S. Xu, Y.-J. Yan, R. Yin, W. Xia, S. Fang, Z. Chen, Y. Li, W. Yang, Y. Guo, and D.-L. Feng, Multiband Superconductivity with Sign-Preserving Order Parameter in Kagome Superconductor CsV_3Sb_5, Phys. Rev. Lett. **127**, 187004 (2021).

[60] W. Duan, Z. Nie, S. Luo, F. Yu, B. R. Ortiz, L. Yin, H. Su, F. Du, A. Wang, Y. Chen *et al.*, Nodeless superconductivity in the kagome metal CsV_3Sb_5, Sci. China: Phys., Mech. Astron. **64**, 107462 (2021).

[61] C. C. Zhao, L. S. Wang, W. Xia, Q. W. Yin, J. M. Ni, Y. Y. Huang, C. P. Tu, Z. C. Tao, Z. J. Tu, C. S. Gong *et al.*, Nodal superconductivity and superconducting domes in the topological kagome metal CsV_3Sb_5, arXiv:2102.08356.

[62] Z. Liang, X. Hou, F. Zhang, W. Ma, P. Wu, Z. Zhang, F. Yu, J.-J. Ying, K. Jiang, L. Shan, Z. Wang, and X.-H. Chen, Three-Dimensional Charge Density Wave and Surface-Dependent Vortex-Core States in a Kagome Superconductor CsV_3Sb_5, Phys. Rev. X **11**, 031026 (2021).